Development, Integration, and Flight Testing of a Silicon Carbide Propulsion Drive for a Hybrid Electric Aerospace Application

Chris Farnell, *Senior Member, IEEE*, Anna Corbitt, *Graduate Student Member, IEEE*, Wesley G. Schwartz, *Graduate Student Member, IEEE*, Asif Faruque, *Member, IEEE*, Yue Zhao, *Senior Member, IEEE*, David Huitink, *Senior Member, IEEE*, Nenad Miljkovic, *Member, IEEE*, and H. Alan Mantooth, *Fellow, IEEE*

***Abstract*—This article details the design, development, and successful flight testing of an 800 V, 250 kW silicon carbide (SiC) inverter built for a hybrid-electric aircraft propulsion system. Using custom 1200 V SiC modules with pin-fin baseplates and integrated CMOS gate drivers, the inverter achieves high performance and reliability, while a direct cooling approach yields a high power density of approximately 60 kW/L and 30 kW/kg. Addressing key challenges in aerospace electrification, such as thermal management and system reliability in flight environments, the inverter underwent simulations, hardware-in-the-loop testing, and real-world validation. This work culminated in a flight demonstration of an experimental hybrid electric aircraft. This first university-developed SiC propulsion flight, recognized with an R&D 100 award, underscores the role of SiC technology in the advancement of hybrid-electric aviation efficiency and sustainability.**

***Index Terms*—Controller hardware-in-the-loop (cHIL) testing, electric aircraft, embedded systems, flight qualification, reliability, silicon carbide (SiC) inverter.**

I. Introduction

THE global transportation sector is undergoing a transformative shift toward electrification, driven by the urgent need to reduce greenhouse gas emissions and reliance on fossil fuels. While electric vehicles (EVs) have gained significant traction in the automotive industry, there is growing interest in extending electrification to aerospace applications [1], [2]. The aviation industry is a major contributor to carbon emissions, accounting for approximately 2% –3% of global CO_2 emissions, with projections indicating a continued rise in air travel demand [3], [4], [5]. Consequently, there has been an increasing focus on the development of more efficient and environmentally sustainable propulsion systems for aircraft [6].

Recent research efforts in transportation electrification have emphasized improving the efficiency, power density, and reliability of electric propulsion systems for aviation applications [7]. The primary goal is to minimize fuel consumption and environmental impact, while maintaining or enhancing flight performance. High power density and system miniaturization are particularly critical in aerospace applications, where weight and space constraints directly affect payload capacity and operational range. Advancements in power electronics, electric machines, and energy storage technologies have accelerated the feasibility of electric and hybrid-electric aircraft [8], [9], [10].

Although full electrification of aircraft remains an objective, hybrid-electric propulsion has emerged as a promising interim solution. Hybrid-electric aircraft integrate electric propulsion with conventional combustion engines or other technologies, leveraging the benefits of both. This approach enables a significant reduction in fuel consumption and emissions without compromising the aircraft's range or operational feasibility. Various research initiatives have explored hybrid-electric configurations, including parallel and series hybrid architectures, each offering distinct tradeoffs in efficiency, power management, and integration complexity [3], [11].

Small planes, such as the Cessna 337 could benefit from a transition to a hybrid electric topology. These planes are typically used as air taxis in island regions and other remote areas. Traditionally, this type of aircraft has two gasoline-powered engines that drive the propulsion system. These types of combustion engines are known for their high fuel consumption rates. The overall fuel consumption could be significantly reduced by replacing one of the two gasoline-powered engines with an electric motor [12]. For example, the experimental aircraft in this article, shown in Fig. 1, utilizes a front-combustion engine with a fully electric rear motor to demonstrate this concept.

A critical component of a hybrid-electric aircraft is the power electronics system, which governs energy conversion and motor

Received 5 April 2025; revised 1 July 2025; accepted 1 August 2025. Date of publication 11 August 2025; date of current version 8 September 2025. This work was supported by the Advanced Research Projects Agency Energy (ARPA-E), U.S. Department of Energy, under Award DE-AR0000895. Recommended for publication by Associate Editor O. Lucia. *(Corresponding author: Chris Farnell.)*

Chris Farnell, Anna Corbitt, Wesley G. Schwartz, Asif Faruque, Yue Zhao, David Huitink, and H. Alan Mantooth are with the Department of Electrical Engineering and Computer Science, University of Arkansas, Fayetteville, AR 72701 USA (e-mail: cfarnell@uark.edu; amcorbit@uark.edu; wgschwar@uark.edu; kafaruqu@uark.edu; yuezhao@uark.edu; dhuitin@uark.edu; mantooth@uark.edu).

Nenad Miljkovic is with Mechanical Science and Engineering, University of Illinois at Urbana-Champaign, Urbana, IL 61801 USA (e-mail: nmiljkov@illinois.edu).

Color versions of one or more figures in this article are available at https://doi.org/10.1109/TPEL.2025.3597905.

Digital Object Identifier 10.1109/TPEL.2025.3597905

control [13]. Silicon carbide (SiC)-based inverters have demonstrated superior efficiency, higher switching frequencies, and reduced thermal losses compared to traditional silicon (Si)-based inverters, making them well-suited for aerospace applications. For example in [14], the author demonstrates the benefits of using SiC MOSFETs in place of Si IGBTs for aerospace applications with the main drawback of the SiC devices being the cost. However, designing motor drive systems that use SiC devices also has its challenges. The authors in [15] discuss the challenge of ac common-mode currents in SiC inverters due to the high dv/dt environment and propose a staggered PWM scheme to minimize such peak AC common-mode currents. Research using SiC components plays a crucial role in electrifying the aerospace industry by enhancing performance, longevity, and aiming to improve cost competitiveness in the future.

This article presents the design, development, and experimental validation of an 800 V 250 kW SiC-based inverter to power the rear electrical motor in a hybrid electric aircraft testbed developed by Ampaire Inc., an electrified aircraft company in Southern California [16]. Designed to drive a 200 kW permanent magnet synchronous machine (PMSM), the inverter plays a key role in reducing fuel consumption by enabling electric propulsion during cruising phases and reserving conventional engine operation for demanding tasks, such as takeoff and acceleration. A direct cooling mechanism was developed to enable power density close to 60 kW/l and 30 kW/kg. The inverter was developed and tested at the University of Arkansas' 6 MVA test facility, the National Center for Reliable Electric Power Transmission (NCREPT) [17], as part of an industry-academic collaboration between the University of Arkansas, the University of Illinois Urbana-Champaign, Ampaire Inc., and Wolfspeed Inc.

In terms of aircraft applications, reliability, and safety are some of the main concerns due to the operational environment of an aircraft. An electric propulsion system is comprised of a significant number of power electronic components, and it is crucial to ensure the reliability and thermal management of those devices [18]. In this work, the developed traction inverter was subjected to comprehensive testing to ensure safety and meet federal aviation administration (FAA) qualifications. A detailed system-level functional hazards assessment (FHA) was determined for the developed inverter. After FAA certification, the inverter was installed in Ampaire's experimental aircraft, and a successful test flight was completed in February 2023. Though there have been numerous works on the development of SiC inverters for electric and hybrid electric aircraft such as [19], [20], [21], [22], and [23], it is very rare to see an actual in-flight demonstration of the SiC propulsion drives. In fact, this work received an R&D 100 award for being the first ever flight of a university-developed propulsion system [24].

The rest of this article is organized as follows. Section II discusses the integrated gate driver design. Section III describes the thermal management. Section IV presents the controller development and simulation, while Section V describes inverter reliability considerations. Section VI details the hardware testing at the university facility. Section VII presents the successful flight test. Finally, Section VIII concludes this article.

Fig. 1. Hybrid electric aircraft flight testing with experimental inverter installed.

Fig. 2. 4H-SiC wafer having the planar CMOS gate drivers fabricated.

II. Design and Integration of CMOS Gate Drivers

In this work, single-chip gate drivers are designed and fabricated on planar SiC CMOS process technology to take full advantage of the SiC circuit topologies, as conventional Si gate drivers cannot withstand the high junction temperature within the module [25]. Those gate drivers are then integrated within the commercial SiC power modules to reduce gate loop inductance, lessen the gate oscillation stress on the SiC power device gate oxide, and take a further step toward increased power density. The design, fabrication, and integration of SiC gate drivers inside a commercial SiC power module are presented in this section. The SiC gate drivers were fabricated on a 1-μm 4H-SiC CMOS process, which comes with a single metal layer and a single poly layer. A compact model, BSIM4SIC, was developed and implemented for the n-type and p-type lateral 4H-SiC MOSFETs to facilitate gate driver circuit design and simulation in the Cadence virtuoso environment [26]. The current drive for this planar SiC CMOS process is, however, lower than that of its Si counterparts because the process is still in its infancy. Also, in contrast to Si, the planar SiC process' current drive capability rises with temperature up to 225 °C –275 °C due to the increase in thermally generated carriers, where these carriers have not yet reached a density that prevents carrier mobility [27]. The SiC gate drivers were designed to be integrated inside commercial SiC power modules from Wolfspeed. The target specifications of the source and sink current are approximately 2 A. These specifications were synthesized based on the available area of approximately 6 mm^2 inside the module and the achievable

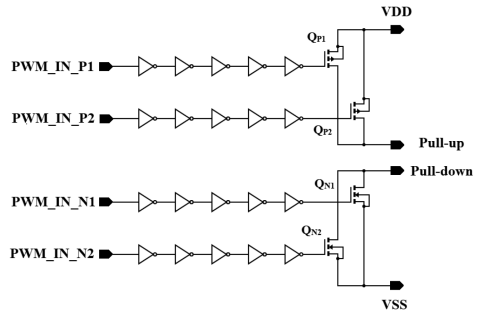

Fig. 3. Schematic diagram of the SiC gate driver.

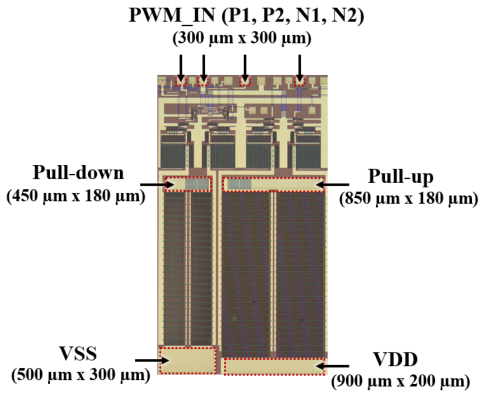

Fig. 4. Fabricated SiC gate driver die micrograph labeling the input and power supply bond pads. Total die area 3 mm × 5 mm.

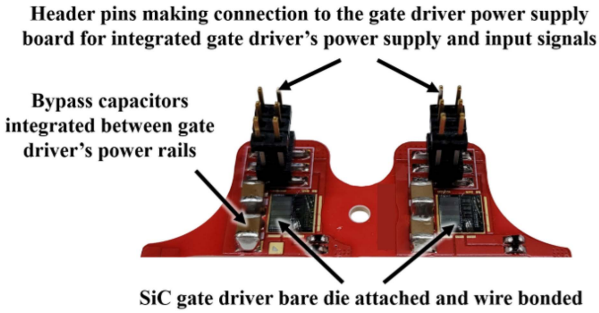

(a)

(b)

Fig. 5. (a) High-temperature printed circuit board (PCB) containing the SiC gate driver bare die and other passives for module integration. (b) SiC IGDM.

transistor drive currents from the SiC process utilizing this area. The gate driver has two key stages, as shown in Fig. 3. The first stage consists of inverter-based buffer chains, and the second stage has PMOS and NMOS devices in a totem-pole buffer connection. In total, there are two PMOS and two NMOS transistors in the second stage. Each PMOS in the second stage acts as the pull-up device, and conversely, each NMOS acts as the pull-down device. Each of these devices can be activated individually through the buffer chain. In this design, the pull-up and pull-down outputs were separated to facilitate different gate resistors, if desired. The first-stage inverter buffer chain was designed using PMOS and NMOS devices with a channel length of 1.5 μm, while the PMOS and NMOS devices in the totem-pole second stage have a channel length of 1.2 μm (see Fig. 2). The fabricated die micrograph, along with the pad dimensions and placements, are shown in Fig. 4. The bond pads and layout orientation were configured for wire bonding within the HT-3292-R-VB SiC power module from Wolfspeed.

The SiC gate drivers are designed to be integrated inside commercially available HT-3292-R-VB SiC modules manufactured by Wolfspeed. The module contains two switch positions in the half-bridge configuration. 5(a) shows the high-temperature PCB that accommodates the two SiC gate driver die for each switching position and other passives inside the module. The bare die are attached to the exposed pads on the PCB through a high-temperature adhesive. The 25 μm Al wirebonds are then used to bond the die pads to the landing pads on the PCB, establishing connections for gate driver power supply, input, and output signals. From those landing pads through PCB traces, the gate driver power supply and input signals are terminated into the header pins, and the gate driver output signals are distributed across the module base, making connections to the power die. In order to prevent the full exposure of the power die arrangement within the SiC power module and preserve Wolfspeed's intellectual property (IP) only the relevant portion of the PCB outlining the UA's SiC gate driver integration is shown in 5(a). For each gate driver power supply, 2.2 μF high-temperature ceramic capacitors are placed between the gate driver power rails and integrated into the module to provide a strong local power supply domain for the gate drivers. The PCB is, then, safely hidden behind the module case. Fig. 5(b) shows the half-bridge SiC integrated gate driver module (IGDM). From a user's perspective, it is identical to a conventional HT-3292-R-VB module. However, the header pins on the left do not have the same configuration as a conventional module. Instead, these pins are replaced by the integrated gate driver's power supply and input signal pins. In order to provide the necessary isolation for the integrated gate driver's power supply and input signals, an external gate driver power supply board is required. This gate driver power supply board receives the PWM input signals for the half-bridge SiC IGDM from the controller and, with proper isolation, operates the SiC IGDM while being connected with the module through the header pins.

Extensive double pulse tests (DPT) were performed to extract the switching energies of these SiC integrated gate driver modules with a maximum Vds of 900 V and a peak current of 300 A [28]. The results are then compared with the conventional HT-3292-R-VB SiC module driven by an external commercial Si gate driver. Fig. 6 shows the DPT results at 175 °C junction temperature, the maximum recommended operating

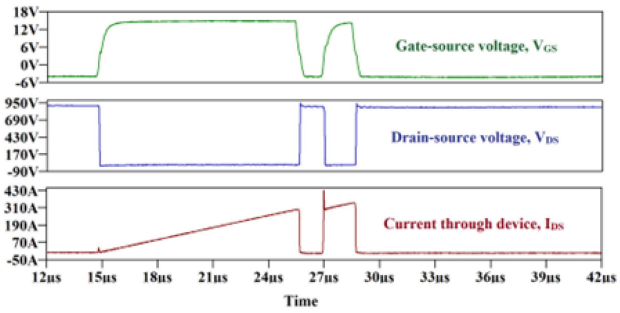

Fig. 6. DPT results at 175 °C junction temperature with maximum Vds of 900 V and peak current of 300 A for SiC IGDM.

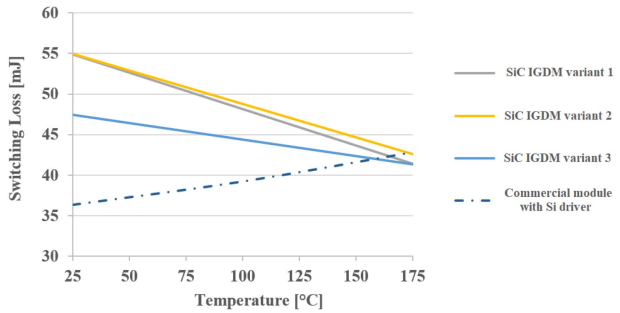

Fig. 7. Switching energies vs. temperature under 900 V, 300 A DPT conditions for multiple SiC integrated gate driver modules and a conventional SiC module driven by external commercial Si gate driver.

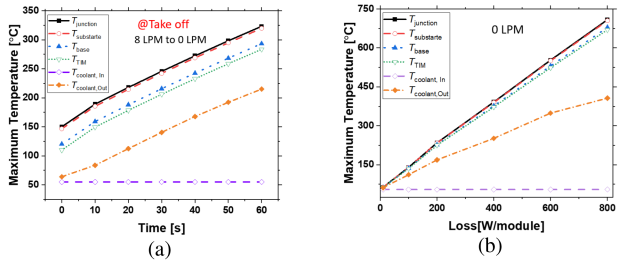

Fig. 8. (a) Icepak simulated thermal profile of three XM3 modules integrated on a cold plate with 8 LPM flow rate during takeoff and rapidly transitioning to 0 LPM. (b) At takeoff loss was 800 W/module and during cruise loss was 200 W/module. Cold plate WEG (50% mixture) was supplied at 55 °C.

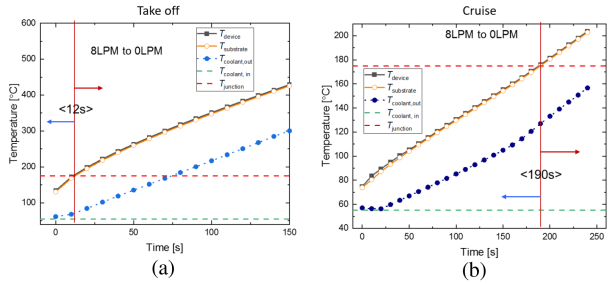

Fig. 9. Transient thermal response of direct cooled system assembly during (a) takeoff and (b) cruise. Transient thermal analysis was performed considering sudden flow shutdown in both take off and cruise condition.

temperature for the SiC power module, with a maximum Vds of 900 V and a peak current of 300 A. While the designed discrete SiC gate driver die can function at much higher temperatures, the SiC modules themselves are at a significant risk of failure if operating beyond 175 °C during the rated DPT test.

Different gate driver design variants, primarily taking the channel length and number of output stages into account, were used to construct multiple SiC integrated gate driver modules. All of those SiC integrated gate driver module variants were put through repeated DPT, and the switching energies against temperatures were noted, as Fig. 7 summarizes. Because SiC gate drivers can drive more current at higher temperatures, the switching losses of the SiC integrated gate driver modules decrease. For the traditional SiC modules driven by external, commercial Si gate drivers, the opposite trend is seen. Indeed, there is a crossover temperature where the SiC integrated gate driver modules outperform the traditional SiC modules, and it occurs just above 150 °C. This crossover temperature is expected to be lowered with further advancements in low-voltage planar CMOS SiC device fabrication technology, allowing low-loss SiC modules at a modest junction temperature.

III. Inverter Thermal Management

Transient thermal analysis of the inverter system was performed using ANSYS and Icepak. Each Wolfspeed XM3 module was considered with a heat loss of 800 W (assuming power losses at takeoff), which were integrated with a commercial-off-the-shelf cold plate. 50% volumetric mixture of water–ethylene glycol (WEG) was supplied to the cold plate at an inlet temperature of 55 °C. For transient analysis, coolant flow rate was reduced from 8 LPM to 0 LPM, and maximum temperature of each stack layer was modeled as a function of time. As shown in Fig. 8(a), within 10 s of flow shut down, the maximum temperature of the modules crosses the junction temperature (>175 °C). As shown in Fig. 8(b), to keep the system temperature under the preferable operating range, inverter power should cut down to approximately 30 kW with 100 W loss per module. Steady state thermal modeling was performed at both takeoff and cruise condition for maximum flow (8 LPM) and no flow (0 LPM) case. In opposite to the regular XM3 module, the finned XM3 module removes the thermal interface layer and allows direct cooling with reduced thermal resistance thus better heat transfer performance. Compared to previously reported results for regular assembly, the direct cooled module reduces the system temperature up to 15 °C (takeoff). Moreover, direct cooling provides additional thermal benefit in case of sudden flow shut down. To model these phenomena, first the system was allowed to run at highest coolant flow rate of 8 LPM and after reaching thermal steady state, the coolant flow was reduced to 0 LPM. This transient thermal analysis was performed for both take-off and cruise condition. For regular XM3 module, during takeoff, system reaches the junction temperature after 6 s of flow loss. Whereas, as shown in Fig 9(a), in case of direct cooling, the system needs ∼12 s to reach the junction temperature (175 °C), which allows 50% more time to derate the inverter power if the pump malfunctions (no flow). Due to lower thermal load at cruise condition, the system needs

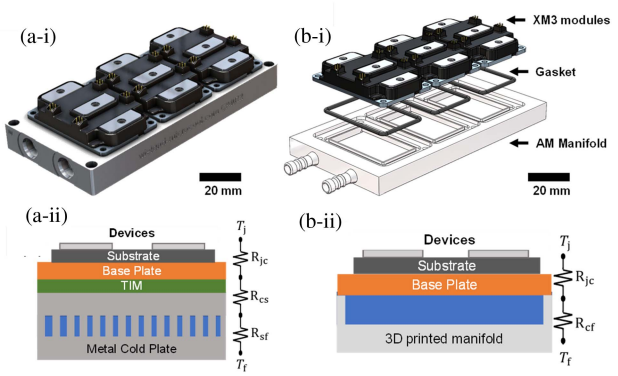

Fig. 10. (a-i) Photograph of the conventional thermal management approach of SiC Wolfspeed XM3 half-bridge power modules using a high-performance all-aluminum cold plate developed by Wieland. (b-i) 3-D exploded view of the thermal management approach using a polymer (white color) additively manufactured coolant manifold and gaskets to mount the XM3 modules. Thermal resistance stackup for the (a-ii) SOA metal cold plate showing the junction-to-case (R_jc), thermal interface (R_cs) and cold plate (R_sf) thermal resistance components. Schematic not to scale. Thermal resistance stackup for the (b-ii) polymer AM manifold showing the junction-to-case (R_jc) and case-to-fluid (R_cf) thermal resistances. Schematic not to scale.

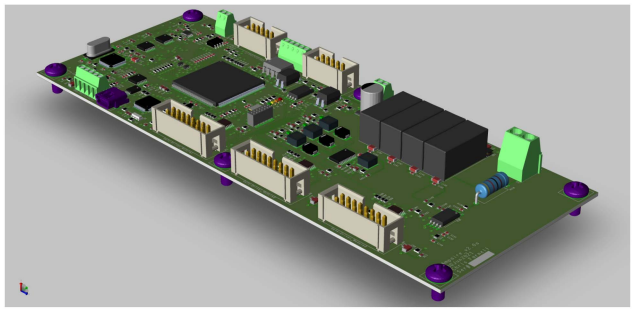

Fig. 11. Isometric 3-D model of custom controller PCB [16].

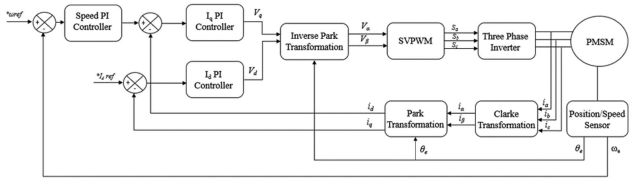

Fig. 12. Field oriented control (FOC) algorithm block diagram [29].

~3 min to cross the junction temperature as shown in Fig. 9(b). The overall thermal management approach for this project is shown in Fig. 10.

The commercial cold plate used in both the model and the experiment is the Weiland 4000 series cold plate. The fins are approximately 0.5 mm in diameter and 4 mm in height, with a design of around 20 FPI (fins per inch) using patented MDT (MicroDeformation Technology). In our modeling approach, the electrical team provided the power loss per module. These losses were distributed equally among the die locations. However, due to flow maldistribution, the actual temperature at each die may vary. For example, during takeoff, the loss per module was 750 W. With 10 dies per module, we allocated a thermal load of 75 W per die. However, in the simulation, because of pressure drop across the flow path, modules located farther from the inlet typically experienced greater pressure drops. As a result, dies at those locations exhibited higher temperatures. For all simulations, a fixed inlet temperature of 55 °C is used for the coolant. The ambient temperature is then the temp at which this coolant rejects heat. The researchers assume that the coolant is at uniform inlet temperature and when the flow is turned OFF, there is no flow and the fluid heats up. A 50/50 mixture of WEG coolant was used in the model.

The calculated power density of approximately 60 kW/L and 30 kW/kg does include the cold plate and the coolant, but not the chiller and radiator, which is taking that heat and rejecting it into the air. This is common practice as the aircraft's heat rejection system is installed regardless of the use of engine type.

IV. Controller Development and Testing

The electric motor selected to replace one of the internal combustion engines on the Cessna 337 aircraft under test was an interior permanent magnet (IPM) PMSM. This selection was based on the lack of brushes, high power density, and the reduced electromagnetic interference (EMI) associated with this type of motor. To drive a PMSM, the user must precisely control the angle between the rotor magnetic field and the magnetic field generated using the stator winding. In order to accomplish this, the authors selected a FOC algorithm based on the TI application note [29]. A custom (PCB) was developed for this project, shown in Fig. 11, to accommodate the numerous communication, safety, and sensor feedback requirements for flight testing.

The researchers utilized a customized resolver feedback circuit to precisely determine both rotor position and speed. The motor currents were then measured and used to execute the Clarke and Park transformations to provide the required direct and quadrature current signals. Once the signals had been transformed into the dq reference frame, standard PI controllers were used for control. Finally an inverse Park transformation was executed and used to generate space vector pulsewidth modulated (SVPWM) signals that provide input to the gate drivers. Fig. 12 shows the basic functions used for the control of this motor. In addition to these motor control functions, the researchers also were required to generate telemetry data for both experimental analysis as well as operational situational awareness. Finally, specifications were established that required multiple warning and fault signals to be routed to the aircraft's primary supervisory, control, and data acquisition systems to ensure safety of all interconnected systems during flight testing.

In order to thoroughly test all operational functions prior to in-lab hardware testing, the authors utilized the Typhoon-HIL real-time simulation platform. This real-time simulation platform allowed the researchers to model the Power Electronics, PMSM, and load profiles with the physical controller connected to the system, shown in Fig. 13. The control board received all the analog signals, such as voltages, currents, and resolver data, from the real-time simulator while the researchers were

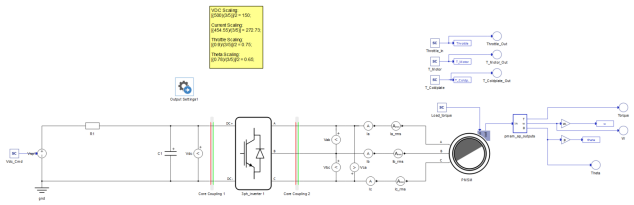

Fig. 13. Typhoon-HIL real-time emulator modeling and cHIL testing.

able to communicate with the controller over the controller area network protocol to send commands and monitor operations. This allowed the researchers the ability to tune most of the operational parameters of the system using the virtualized environment and test all of the equipment and personnel safety functions prior to moving to physical hardware testing. For more information regarding the rapid prototyping efforts, please see [16].

V. Inverter System Reliability Consideration

As electrified passenger aircraft advance toward technical readiness and widespread adoption, reliability becomes a principal consideration for ensuring the safety and longevity of propulsion systems. The automotive industry has paved the way toward expanding standards around reliability qualification for meeting the demands of drivetrain electronics, though it has been principally derived from older automotive electronics standards, such as AEC Q100 and AEC Q101 [30]. AEC's approach to "grading" electronics criticality offers some superiority to more generic reliability qualifications intended for consumer electronics (e.g. JEDEC JESD47 and IPC board level certifications [31], [32]). However, even in these higher graded qualification stresses, most do not encompass the higher operational Tj's seen in modern power electronics modules. For instance grade 0 temperature cycling may include – but not necessarily demand – cycling up to 175 °C, which is the rated Tj of many Si IGBT and SiC MOSFET power modules. Typically, a qualification stress should exceed the operational conditions, and this barely meets the expected operational ratings. At the same time, accelerated testing design can become much more complicated, when considering the variety of stresses that may be experienced at the module level as compared to discrete device temperatures, etc. Consequently, as the criticality of an inoperable drive train on an aircraft intensifies as compared to its land-based vehicular counterparts, the need for renewed scrutiny of qualification strategies has emerged. In the case of the hybrid electric drivetrain developed in this effort, the natural redundancy between electric and gasoline engine power helps to alleviate some of the burden of flight-ready certification; but even still, the FAA requires a variety of preflight demonstrations for proving the robustness of the electric propulsion system under aviation-relevant conditions. For example, the electric drivetrain (particularly the novel SiC-based inverter, in this case) was prescribed for cooling with a max coolant temperature of 55 °C (WEG), while supporting the power requirements for takeoff, which together defines the temperature response of the inverter components (SiC modules, dc link capacitors, gate drive circuitry, etc). Consequently, the development and deployment of the 'all SiC traction inverter system" was accompanied by a series of finite element modeling activities and accelerated testing of the components and inverter system to be flight-ready.

As a somewhat unique operational environment for aircraft, the accelerations (g's) experienced during takeoff and landing, and the vibrations associated with flights represent a reliability risk to PCB assemblies and inverter sub-assemblies. Due to the opportunity for somewhat flexible materials and connectors to bend under acceleration, this can place solder joints, terminals, and other connectors under strains that can drive fractures or fatigue failure. To minimize this risk, there are a number of strategies that generally serve to stiffen the flexural response so that stresses do not concentrate on critical electrical interconnects. In the case of the hybrid inverter system, it was determined that the controller board represented the most pertinent "shock and vibration" risk, due to its relatively long board dimensions and variety of components mounted to it. Of course, the simplest solution to stiffening of the board assembly is to include numerous mounting locations to a stiff plate (e.g. metal housing, etc). However, incorporating mounting holes on a PCB also consumes board real estate, and moreover, the minimization of weight of the mounting plate is desired for overall specific power (kW/kg) maximization. To optimize the board response for minimized risk of component failure in high g acceleration, while maintaining a lowest possible weight, a design optimization was performed for weight minimization, while maintaining the board strain response under a critical level. Based on opportunistic placement of mounting holes on the PCB due to available space in a condensed assembly, the resultant mounting plate of 1/16" Aluminum plate consisted of a frame-like structure with cutouts for weight reduction, which provided the adequate stiffness to maintain satisfactory stress/strain conditions at critical locations on the board – namely, the Ball Grid Array controller processor package interconnects. For comparison, the board was modeled with and without the frame to stiffen its response, in which the frame, shown in Fig. 14, reduced the critical strains to 20% of the board-only mounting to the inverter housing. The subsequent shock and vibration testing was performed in a highly accelerated life testing (HALT) chamber using the fixture suspended on the shaker table in a paired manner with the inverter mounting condition inside the inverter enclosure. A series of drop events at 20, 50, and 60 g's were performed followed by functional testing and visual inspection of any potential damage.

Having successfully passed shock and vibration testing of the controller board, results shown in Fig. 15, – confirming controller functionality after the accelerated tests – the inverter was then required to be validated in a holistic manner. To do so, the entire inverter assembly was constructed and mounted inside of the HALT chamber, shown in Fig. 16, for performing continuous operation during multiaxis shock events. A prescribed acceleration of 6 g's with an 11 ms duration (shock profile provided in was performed 3x for 6 orientations (± X, ± Y, ± Z) for the entire inverter assembly in addition to a powered operation of the inverter during random vibration exposure, Fig. 17. These proved successful without impact to functionality, which cleared the pathway to in-aircraft tests at Ampaire.

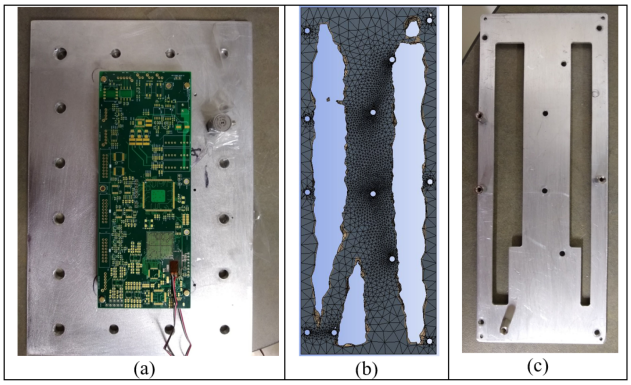

Fig. 14. Shock and vibration analysis of (a) controller board and mounting fixture. (b) topology optimized mount. (c) as-manufactured mount for simplicity of fabrication.

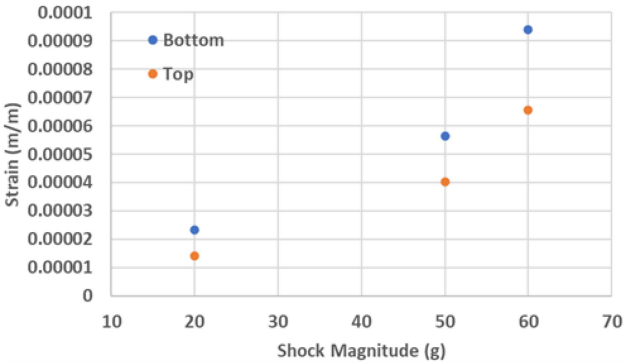

Fig. 15. Shock and vibration testing strain response data measured on top and bottom of custom controller board.

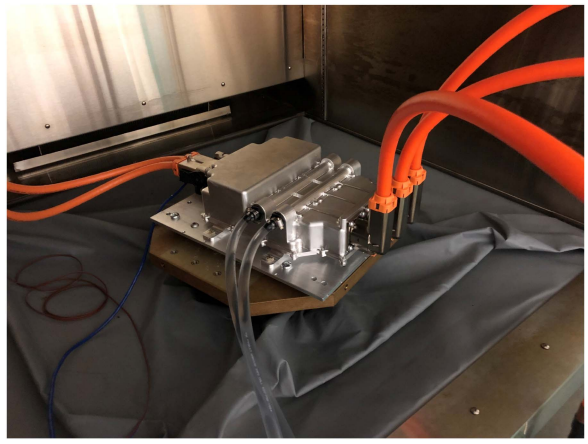

Fig. 16. Shock and vibration testing of fully assembled SiC Inverter while powered on at rated voltage.

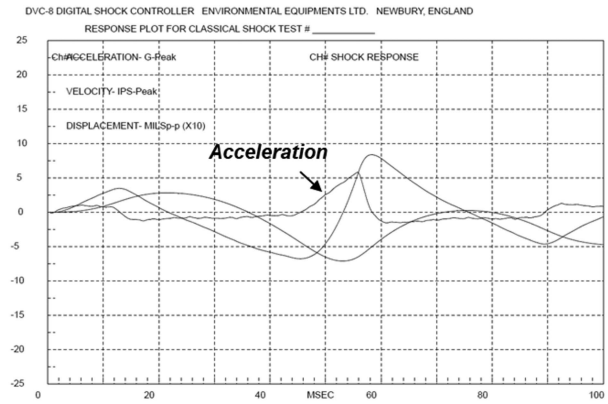

Fig. 17. Shock and vibration testing of fully assembled SiC inverter while powered on at rated voltage (excitation commands).

VI. Hardware Testing

The researchers were able to continue on to real-world hardware testing using the 100 kW dynamometer test stand located at the NCREPT. The existing dynamometer test stand was modified to mount the PMSM that would be used in the aircraft propulsion system. Since the mounting was on one of the motor faces, the development of a new L-shaped bracket was required to secure the motor on the developed test stand. In addition, the motor used for the project was an axial flux motor with an external rotor, necessitating the development and machining of a custom shaft coupler to connect the motor to the dynamometer's resolver feedback system. The coupler was designed using Autodesk Fusion^{TM}. The mounting bracket and shaft coupler can be seen in Fig. 19. Once the design was complete, the machining toolpaths were developed and the raw stock material was purchased. The new coupler was machined in-house using NCREPT's Tormach 1100 M CNC machine and the completed coupler is shown in Fig. 18. Once the parts were machined, the test stand was assembled at NCREPT to resemble the full CAD assembly shown in Fig. 19.

The inverter under test was placed in a 600 L thermal chamber and connected to a 55 °C coolant loop, shown in Fig. 22. It was first tested using open-loop controls and a 750 kW resistive load bank to ensure it could operate up to its 250 kW rating. Then the inverter was connected to the aforementioned PMSM and tuned for the specific motor and loads used. During this testing, advanced hi-speed data acquisition and power analyzer equipment was used to ensure proper operation. Once the motor was tuned appropriately, it was run up to full power, and synthetic fault testing was accomplished by reducing both warning and fault setpoints and ensuring safe operations and failure modes. Fault scenarios, such as over-current, over-voltage, and motor over-speed were evaluated. Once the warning threshold is satisfied, the primary flight control screen shows a specific indication of the issue. Subsequently, if a fault condition is detected, the controller would safely disable the inverter and communicate this to the flight control system. The aircraft was developed as a hybrid electric configuration, so even if the electrical motor is disabled it can revert to a standard internal combustion engine as a backup mode of operation. After the researchers were satisfied with all the safety features, communications, and general operations, long-term endurance testing was accomplished. Simulation data was utilized to develop emulated flying schedules, which mimicked worst case scenarios. This worst case scenario was deemed to be takeoff, cruise, and an

Fig. 18. Custom shaft coupler machined at NCREPT using the Tormach 1100 M CNC.

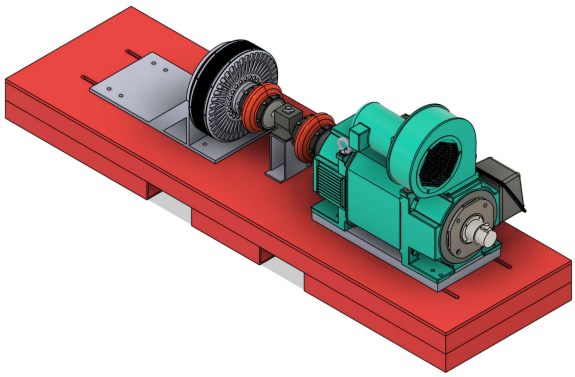

Fig. 19. CAD model of fully assembled, modified Dynamometer test stand at NCREPT used for the initial testing of the silicon carbide traction drive.

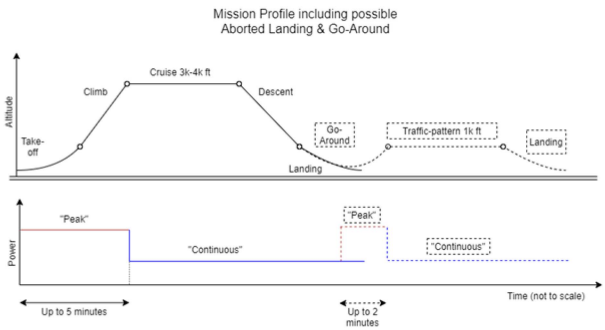

Fig. 20. Mission profile for aircraft flight and ground testing.

immediate turnaround operation. Over the next 8 h, the inverter was run continuously repeating these operations without any breaks, all while the inverter was held at a 55 °C ambient temperature with 55 °C coolant being supplied to the power electronics, shown in Fig. 23. Once these endurance tests were completed successfully, the researchers were able to move on to ground and flight testing onsite at Ampaire's test facilities. Fig. 20 shows the mission profile for flight and ground testing. This profile also incorporates an aborted landing and go-around pattern for worst-case scenarios. The inverter was evaluated

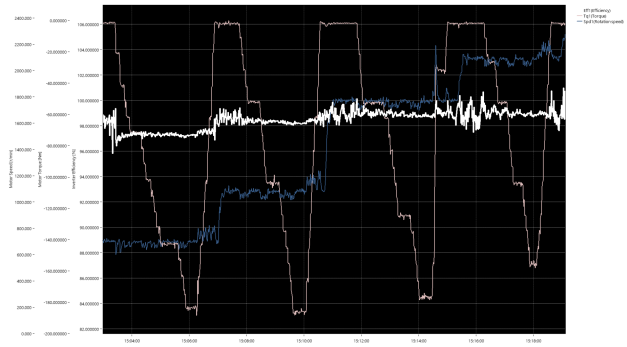

Fig. 21. Inverter speed and torque testing.

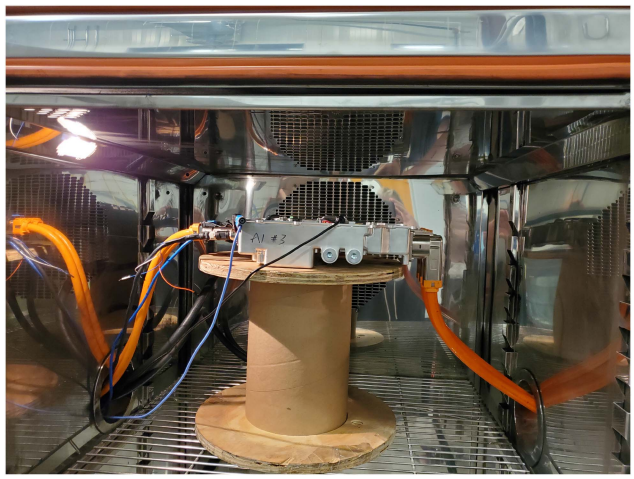

Fig. 22. SiC inverter under test in a thermal chamber.

between speeds from 640 r/min and 2400 r/min and measured inverter efficiencies are between 96% and 98.5% as shown in Fig. 21.

VII. Ground and Flight Testing

The University of Arkansas research team traveled to Ampaire's California headquarters with the SiC Inverter Prototype for field integration and testing. Resolver calibration was required as the motor installed on the experimental aircraft was different from what was used in the laboratory. Once calibration was completed, ground testing was started using an external power supply for safety reasons, this phase of ground testing can be seen in Figs. 24 and 25.

After tuning the resolver, verifying all internal device communications, and the completion of the initial ground testing with the external supply, the airplane's onboard batteries were connected for higher power testing. At this stage of the testing our team ran into an issue with EMI. At the higher power levels, EMI was corrupting the controllers feedback signals and causing the system to enter a fault state. The researchers believed this was a combination of no longer having a bonded connection to ground, as the internal aircraft power supplies had no connection to earth ground, as well as EMI corrupting the gate-driver protection circuits. While differential signaling and

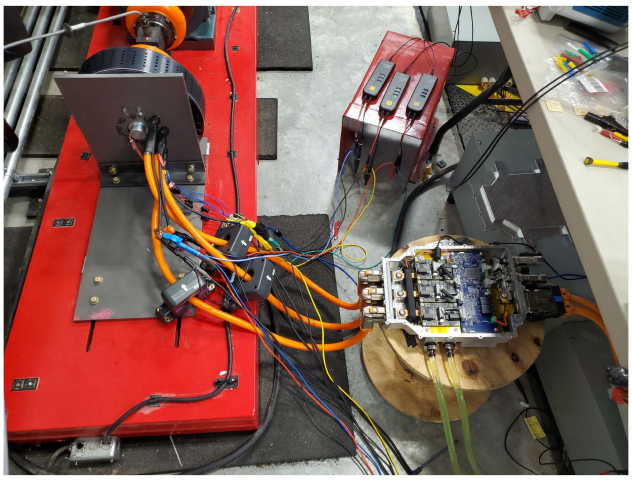

Fig. 23. SiC inverter under test utilizing NCREPT's 100-kW dynamometer [16].

Fig. 24. Final integration of SiC inverter into test airframe.

Fig. 25. Final tuning and ground testing in hangar.

shielding was used in the initial design, additional shielding was incorporated and larger decoupling capacitors were installed on the controller board in the field to mitigate these EMI issues. With the additions of these mitigations, the team was able to operate the SiC inverter up to the target power levels for flight testing. The researchers met with the Ampaire engineering team, as well as with the test pilot to discuss safety and any issues that might prevent a successful flight test. Once this meeting and a subsequent briefing was completed, the test pilot successfully flew the hybrid electric aircraft using primary power from the SiC inverter under test. Fig. 26 shows the experimental aircraft in flight using the SiC inverter discussed in this work.

Fig. 26. Final flight testing of SiC inverter [16].

VIII. Conclusion

The researchers successfully designed, fabricated, and flight tested a 250 kW SiC inverter using an experimental hybrid-electric aircraft. According to the University's industrial and commercial partners, this is a first for a university research team. A novel integrated gate driver was developed for this project to increase overall reliability and power density. Extensive thermal and mechanical analysis was performed to inform the research team's design decisions and ensure strict safety and reliability requirements were met. In addition, the use of rapid prototyping methodologies and controller hardware-in-the-loop (cHIL) resources allowed the research team to meet accelerated requirements and timelines during both the development and testing phases of the custom controller board, algorithms, and safety interlocks. More advanced embedded control resources will be integrated in the future to enable additional capabilities. The future integration of advanced multilevel gate drivers into wide-bandgap device modules will be investigated further. This integration will allow researchers to maximize inverter power densities, while also increasing overall reliability.

Acknowledgment

The views and opinions of authors expressed herein do not necessarily state or reflect those of the United States Government or any agency thereof. This project was developed and tested at the National Center for Reliable Electric Power Transmission (NCREPT), the University of Arkansas High-Power 6 MVA Test Facility. Ampaire Inc. provided technical expertise, project coordination, maintained the experimental airframe, and conducted on airframe ground testing/verification for this project. The researchers would also like to thank Typhoon-HIL for their continued hardware and modeling support. This article was produced by the IEEE Publication Technology Group. They are in Piscataway, NJ.

REFERENCES

[1] B. Sarlioglu and C. T. Morris, "More electric aircraft: Review, challenges, and opportunities for commercial transport aircraft," *IEEE Trans. Transport. Electrific.*, vol. 1, no. 1, pp. 54–64, Jan. 2015.

[2] Federal Aviation Administration, "United States 2021 aviation climate action plan," 2021. Accessed: Mar. 17, 2025. [Online]. Available: https://www.faa.gov/sites/faa.gov/files/2021-11/Aviation_Climate_Action_Plan.pdf

[3] L. Cardone, G. Petrone, S. De Rosa, F. Franco, and C. Greco, "Review of the recent developments about the hybrid propelled aircraft," *Aerotecnica Missili Spazio*, vol. 103, p. 9, 2023.

[4] Environmental and Energy Study Institute, "The growth in greenhouse gas emissions from commercial aviation," 2019. Accessed: Mar. 17, 2025. [Online]. Available: https://www.eesi.org/files/IssueBrief_Climate_Impacts_Aviation_2019rev2022.pdf

[5] S. N. Kumar and D. Rutherford, "Lifetime emissions from aircraft under a net-zero carbon budget," 2024. Accessed: Mar. 17, 2025. [Online]. Available: https://theicct.org/wp-content/uploads/2024/07/ID-188-\%E2\%80\%93-Committed-emissions_wp_final.pdf

[6] P. J. Ansell and K. S. Haran, "Electrified airplanes: A path to zero-emission air travel," *IEEE Electrific. Mag.*, vol. 8, no. 2, pp. 18–26, Feb. 2020.

[7] A. Barzkar and M. Ghassemi, "Electric power systems in more and all electric aircraft: A review," *IEEE Access*, vol. 8, pp. 169314–169332, 2020.

[8] B. Appiah, A. -Gyamfi, and C. Good, "Electric aviation: A review of concepts and enabling technologies," *Transp. Eng.*, vol. 9, 2022, Art. no. 100134.

[9] Y. Liang, G. R. C. Mouli, and P. Bauer, "Charging technology for electric aircraft: State of the Art, trends, and challenges," *IEEE Trans. Transport. Electrific.*, vol. 10, no. 3, pp. 6761–6788, Mar. 2024.

[10] A. Misra, "Energy storage for electrified aircraft: The need for better batteries, fuel cells, and supercapacitors," *IEEE Electrific. Mag.*, vol. 6, no. 3, pp. 54–61, Mar. 2018.

[11] S. Sahoo, X. Zhao, and K. Kyprianidis, "A review of concepts, benefits, and challenges for future electrical propulsion-based aircraft," *Aerospace*, vol. 7, no. 4, 2020, Art. no. 44 .

[12] A. Schwab, A. Thomas, J. Bennet, E. Robertson, and S. Cary, "Electrification of aircraft: Challenges, barriers, and potential impacts," 2021. Accessed: Mar. 18, 2025. [Online]. Available: https://www.nrel.gov/docs/fy22osti/80220.pdf

[13] L. Radomsky, R. Keilmann, D. Ferch, and R. Mallwitz, "Challenges and opportunities in power electronics design for all- and hybrid-electric aircraft: A qualitative review and outlook," *CEAS Aeronautical J.*, vol. 15, pp. 751–764, 2024.

[14] W. Perdikakis, M. J. Scott, K. J. Yost, C. Kitzmiller, B. Hall, and K. A. Sheets, "Comparison of Si and SiC EMI and efficiency in a two-level aerospace motor drive application," *IEEE Trans. Transport. Electrific.*, vol. 6, no. 4, pp. 1401–1411, Apr. 2020.

[15] R. Phukan, X. Zhao, P. Asfaux, D. Dong, and R. Burgos, "Investigation of staggered PWM scheme for ac common mode current minimization in sic-based three-phase inverters," *IEEE Trans. Transport. Electrific.*, vol. 8, no. 4, pp. 4378–4390, Apr. 2022.

[16] C. Farnell, J. Jackson, A. Corbitt, and H. A. Mantooth, "Rapid prototyping of a SiC-based PMSM motor drive for aerospace applications," in *Proc. 2023 IEEE Des. Methodol. Conf. (DMC)*, 2023, pp. 1–5.

[17] A. Corbitt, W. G. Schwartz, C. Farnell, J. C. Balda, and A. Mantooth, "The national center for reliable electric power transmission test facility," *IEEE Open J. Power Electron.*, vol. 5, pp. 754–764, 2024.

[18] C.-W. Chang et al., "Thermal consideration and design for a 200-kw sic-based high-density three-phase inverter in more electric aircraft," *IEEE Trans. Emerg. Sel. Topics Power Electron.*, vol. 11, no. 6, pp. 5910–5929, Jun. 2023.

[19] S. Yin, K. J. Tseng, R. Simanjorang, Y. Liu, and J. Pou, "A 50-kw high-frequency and high-efficiency sic voltage source inverter for more electric aircraft," *IEEE Trans. Ind. Electron.*, vol. 64, no. 11, pp. 9124–9134, Nov. 2017.

[20] A. Nawawi et al., "Design and demonstration of high power density inverter for aircraft applications," *IEEE Trans. Ind. Appl.*, vol. 53, no. 2, pp. 1168–1176, Feb. 2017.

[21] Z. Wang, Y. Wu, M. H. Mahmud, Z. Zhao, Y. Zhao, and H. A. Mantooth, "Design and validation of a 250-kw all-silicon carbide high-density three-level t-type inverter," *IEEE Trans. Emerg. Sel. Topics Power Electron.*, vol. 8, no. 1, pp. 578–588, Jan. 2020.

[22] X. Zhao et al., "Design of ultracompact gate driver integrated with current sensor and commutation path for a 211-kw three-level sic aircraft propulsion inverter," *IEEE Trans. Emerg. Sel. Topics Power Electron.*, vol. 11, no. 4, pp. 4077–4094, Apr. 2023.

[23] X. Zhao et al., "Design and implementation of SiC-based 200-kw high-density high-speed high-altitude electric propulsion ac drive system," *IEEE Trans. Emerg. Sel. Topics Power Electron.*, vol. 12, no. 5, pp. 5176–5199, May 2024.

[24] R&D Magazine, "R&d 100 winners for 2023 are announced," 2023. Accessed: Mar. 17, 2025. [Online]. Available: https://www.rdworldonline.com/rd-100-winners-for-2023-are-announced-2/

[25] H. Wang et al., "A review of silicon carbide CMOS technology for harsh environments," *Mater. Sci. Semicond. Process.*, vol. 178, 2024, Art. no. 108422.

[26] A. S. M. K. Hasan et al., "Temperature scaling and C–V modeling of SiC low-voltage MOSFETs for IC design," *IEEE Trans. Emerg. Sel. Topics Power Electron.*, vol. 13, no. 1, pp. 335–347, Jan. 2025.

[27] A. S. Kashyap et al., "Silicon carbide integrated circuits for extreme environments," in *Proc. 1st IEEE Workshop Wide Bandgap Power Devices Appl.*, 2013, pp. 60–63.

[28] Z. Zhang, F. Wang, L. M. Tolbert, B. J. Blalock, and D. J. Costinett, "Evaluation of switching performance of SiC devices in PWM inverter-fed induction motor drives," *IEEE Trans. Power Electron.*, vol. 30, no. 10, pp. 5701–5711, Oct. 2015.

[29] R. Ramamoorthy, B. Larimore, and M. Bhardwaj, "Sensored field oriented control of 3-phase permanent magnet synchronous motors using tms320f2837x," 2021.

[30] Automotive Electronics Council, "Aec documents," 2025. [Online]. Availabel: Mar. 31, 2025 http://www.aecouncil.com/AECDocuments.html

[31] Joint Electron Device Engineering Council, "JEDEC standards and documents," 2025. [Online]. Availabel: Mar. 31, 2025. https://www.jedec.org/document_search?search_api_views_fulltext=JESD47

[32] Institute for Printed Circuits, "IPC certifications," 2025. [Online]. Availabel: Mar. 31, 2025 https://www.ipc.org/ipc-certifications

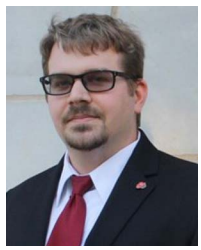

Chris Farnell (Senior Member, IEEE) received the Ph.D. degree in electrical engineering from the University of Arkansas, Fayetteville, AR, USA, in 2020.

He is currently an Assistant Professor with the University of Arkansas's Electrical Engineering and Computer Science (EECS) Department. His research interests include Cybersecurity for Critical Infrastructure, Embedded System Design, FPGA Design, Advanced Control Algorithms, and Power Electronics.

Dr. Farnell is currently serving as an Associate Director for the National Center for Reliable Electric Power Transmission (NCREPT) located at the University of Arkansas. This 12 000-square-foot laboratory provides the equipment, technical staff, and instrumentation to test and evaluate power electronic circuits and systems at realistic industrial and distribution voltage levels up to 6 MVA power ratings. He is the Current Chair for the IEEE Ozark Section, Treasurer for the newly formed IEEE Computer Society Chapter, the CyberHogs Registered Student Organization (RSO) Faculty Mentor, and remains active in K-12 outreach activities.

Anna Corbitt (Graduate Student Member, IEEE) graduated from Murfreesboro High School, AR, USA, in 2017. She received the B.S degree in engineering–physics from Southern Arkansas University, Magnolia, AR, USA, in 2021, and the M.S. degree in electrical engineering in 2023 from the University of Arkansas, Fayetteville, AR, USA, where she is currently working toward the Ph.D. degree in electrical engineering.

In 2023, she was hired as a Full-Time Staff Member with the National Center for Reliable Electric Power Transmission (NCREPT), the University of Arkansas, where she currently works as a Test Engineer. In 2022, she worked with Toyota Research and Development (R&D) in Ann Arbor, MI, USA, as a Summer Design co-op. Her current research interests include power electronics, electric vehicle applications, AI/ML, and embedded systems.

Ms. Corbitt was the recipient of the Distinguished Doctoral Fellowship with the University of Arkansas in 2021..

Wesley G. Schwartz (Graduate Student Member, IEEE) was born in Fort Smith, Arkansas, AR, USA, in 2000. He received the B.S. degree in electrical engineering, in 2022, from the University of Arkansas, Fayetteville, AR, USA, where he is currently working toward the Ph.D. degree in electrical engineering.

In 2023, he was hired as a Full-Time Staff Member with the National Center for Reliable Electric Power Transmission (NCREPT), the University of Arkansas. From 2022 to 2023, he was a Power Systems Engineer with Los Alamos National Laboratory in Los Alamos, NM, USA. His research interests include cybersecurity for critical infrastructure, embedded system design, and power electronics.

Mr. Schwartz was the recipient of the Honors College Fellowship, the Governor's Distinguished Scholarship, and the William E. Bush Endowed Scholarship in Electrical Engineering with the University of Arkansas from 2018 to 2022. He is a Member of Eta Kappa Nu and Tau Beta Pi and is active in K-12 outreach activities.

Asif Faruque (Member, IEEE) received the B.Sc. and M.Sc. degrees in electrical and electronic engineering from the Bangladesh University of Engineering and Technology, Dhaka, Bangladesh, in 2015 and 2018, respectively, and Ph.D. degree in electrical engineering from the University of Arkansas, Fayetteville, AR, USA, in 2024.

He is currently working as a High-bandwidth Memory Design Engineer with Micron Technology, Inc. His research interest includes designing high-temperature mixed-signal integrated circuits for power electronic applications.

Yue Zhao (Senior Member, IEEE) received the Ph.D. degree in electrical engineering from the University of Nebraska-Lincoln, Lincoln, NE, USA, in 2014.

Since 2015, he has been with University of Arkansas, Fayetteville, AR, USA, where he is currently an Associate Professor in electrical engineering. He also serves as the Executive Director for NSF Center on GRid-connected Advanced Power Electronic Systems (GRAPES). He has 4 U.S. patents granted and coauthored more than 180 papers in refereed journals and international conference proceedings.

Dr. Zhao was the recipient of the 2025 John L. Imhoff Outstanding Research Award, the 2020 IEEE Industry Applications Society Andrew W. Smith Outstanding Young Member Achievement Award, and the 2018 NSF CAREER Award.

David Huitink (Senior Member, IEEE) received the B.S., M.S., and Ph.D. degrees in mechanical engineering from Texas A&M University, College Station, TX, USA, in 2006, 2007, and 2011, respectively.

He is an Associate Professor, where he has led productive fundamental and applied research in focusing on the intersection of materials and thermal sciences for applications in electronics with dozens of journal articles, patents and research and collaboration awards. From 2011 to 2016, much of his research builds on his industry experience with Intel, where he supported Intel's ATTD (Assembly/Test Technology Development) in the area of program management of Quality and Reliability for Intel Custom Foundry products.

the Director of the University of Arkansas High Density Electronics Center, and holder of the 21st Century Professorship in mechanical engineering, the University of Arkansas, Fayetteville, AR, USA.

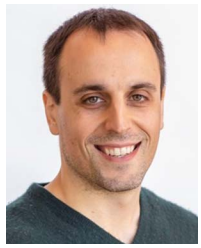

Nenad Miljkovic (Member, IEEE) received the BASc. degree from the University of Waterloo, Waterloo, ON, Canada, in 2009, and M.S. and Ph.D. degrees from the Massachusetts Institute of Technology, Cambridge, MA, USA, in 2011 and 2013, respectively, all in mechanical engineering.

He is currently the Founder Professor of Mechanical Science and Engineering with the University of Illinois, Urbana-Champaign, IL, USA, where he leads the Energy Transport Research Laboratory and directs the Air Conditioning and Refrigeration Center. He has courtesy appointments in Electrical and Computer Engineering, and the Materials Research Laboratory. His research interests include the multidisciplinary fields of thermo-fluid science, interfacial phenomena, and energy.

Dr. Miljkovic was the recipient of the National Science Foundation CAREER Award, the Office of Naval Research Young Investigator Award, the ASME Pi Tau Sigma Gold Medal, and the ASME Bergles-Rohsenow Award. He is a Fellow of the ASME.

H. Alan Mantooth (Fellow, IEEE) received the B.S.E.E. and M.S.E.E. degrees from the University of Arkansas (UA), Fayetteville, AR, USA, in 1985 and 1986, respectively, and the Ph.D. degree from Georgia Institute of Technology (Georgia Tech), Atlanta, GA, USA, in 1990.

He joined the Faculty of the Department of Electrical Engineering with the University of Arkansas, where he is currently a Distinguished Professor. He worked for eight years with Analogy, a startup company in Oregon. His research interests include analog and mixed-signal IC design and CAD, semiconductor device modeling, power electronics, power electronic packaging, and cybersecurity.

Dr. Mantooth established and serves as an Executive Director of the National Center for Reliable Electric Power Transmission (NCREPT). He is a Member of Tau Beta Pi, Sigma Xi, and Eta Kappa Nu, and Registered Professional Engineer in Arkansas. He is the Founding Director of the NSF Industry/University Cooperative Research Center on GRid-connected Advanced Power Electronic Systems (GRAPES) and Deputy Director of the POETS NSF Engineering Research Center. He holds the 21st Century Research Leadership Chair in Engineering. He is a Past-President of the IEEE Power Electronics Society (PELS). He currently serves as an Editor-in-Chief for the *IEEE Open Journal of Power Electronics* and *Division II Director on the IEEE Board of Directors.*